

## CHANDRA OBSERVATIONS OF THE PULSAR WIND NEBULA IN SUPERNOVA REMNANT G0.9+0.1

B. M. GAENSLER,<sup>1,2</sup> M. J. PIVOVAROFF,<sup>1,3</sup> AND G. P. GARMIRE<sup>4</sup>

Received 2001 May 14; accepted 2001 June 26; published 2001 July 16

### ABSTRACT

We present observations with the *Chandra X-Ray Observatory* of the pulsar wind nebula (PWN) within the supernova remnant G0.9+0.1. At *Chandra*'s high resolution, the PWN has a clear axial symmetry; a faint X-ray point source lying along the symmetry axis possibly corresponds to the pulsar itself. We argue that the nebular morphology can be explained in terms of a torus of emission in the pulsar's equatorial plane and a jet directed along the pulsar spin axis, as is seen in the X-ray nebulae powered by other young pulsars. A bright clump of emission within the PWN breaks the axisymmetry and may correspond to an intermediate-latitude feature in the pulsar wind.

*Subject headings:* ISM: individual (G0.9+0.1) — pulsars: general — stars: winds, outflows — supernova remnants

### 1. INTRODUCTION

When a pulsar's relativistic wind is sufficiently confined, a synchrotron-emitting pulsar wind nebula (PWN) is produced (Gaensler 2001). Because of the short synchrotron lifetimes of high-energy electrons, X-ray emission from a PWN directly traces the current energetics of the pulsar. The spectral and morphological characteristics of an X-ray PWN can thus reveal the structure and composition of the pulsar wind and possibly also the orientation of the pulsar's spin axis and/or velocity vector. For a PWN in which no pulsar has yet been detected, this nebular emission is our only insight into the location and energetics of the central source.

At the center of the supernova remnant (SNR) G0.9+0.1 is one of the many PWNs in which no pulsar has yet been seen. This PWN was first identified by its radio emission (Helfand & Becker 1987) but has recently been detected in X-rays using *BeppoSAX* (Mereghetti, Sidoli, & Israel 1998; Sidoli et al. 2000). In these observations, X-ray emission from the PWN has a power-law spectrum with a photon index  $\Gamma = 2.0 \pm 0.3$  (where  $N \propto E^{-\Gamma}$ ), with an unabsorbed flux density  $f_x = 6.6^{+1.3}_{-0.8} \times 10^{-12}$  ergs s<sup>-1</sup> cm<sup>-2</sup> in the energy range of 2–10 keV. The inferred column density is very high,  $N_H = (1.1 \pm 0.2) \times 10^{23}$  cm<sup>-2</sup>, accounting for the lack of any X-ray emission from the surrounding SNR and suggesting an approximate distance of  $\sim 10$  kpc. The size of the SNR shell then implies an age of  $\tau = 1\text{--}7$  kyr (Mereghetti et al. 1998). From the X-ray luminosity of the PWN, Sidoli et al. (2000) estimate that the central pulsar has a spin-down luminosity  $\dot{E} \sim 1.5 \times 10^{37}$  ergs s<sup>-1</sup> and a spin period  $P \sim 80\text{--}190$  ms.

Here we present higher resolution observations of this source with the *Chandra X-Ray Observatory*. This experiment had two aims: to study the morphology of the PWN and to search for emission from the central pulsar.

### 2. OBSERVATIONS AND ANALYSIS

Observations of G0.9+0.1 were made with the Advanced CCD Imaging Spectrometer (ACIS) aboard *Chandra*. ACIS is an array of 10  $1024 \times 1024$  pixel CCDs fabricated by MIT Lincoln Laboratory and is the result of a collaboration between MIT and PSU. These X-ray-sensitive devices have large detection efficiency (10%–90%) and moderate-energy resolution ( $E/\Delta E \sim 10\text{--}50$ ) over a 0.2–10.0 keV passband. The CCDs have a scale of  $0''.492$  pixel<sup>-1</sup>, which is well matched to the on-axis point-spread function (FWHM  $\lesssim 1''$ ). The instrument and its calibration are described in detail by Burke et al. (1997) and Bautz et al. (1998).

A single exposure of length 35 ks was made on 2000 October 27 in the standard “timed exposure” mode, with the aimpoint located at the center of the back-illuminated S3 chip. Data were first processed by the *Chandra* Science Center (ASCDS version R4CU5UPD11.1) and were subsequently analyzed with CIAO v2.1. A brief interval of high background was rejected, resulting in a usable exposure time of 34,741 s. Counts received from energies below 0.5 keV or above 8.0 keV were dominated by background; data meeting these criteria were excluded from subsequent analysis.

X-ray emission from the bright star HD 161507 was detected at the western edge of the S3 chip. The X-ray position measured for this source agrees with the optical position given in the Tycho Reference Catalogue (Høg et al. 1998) to better than  $0''.5$  in each coordinate.

### 3. RESULTS

In Figure 1, we compare a broadband (0.5–8.0 keV) image of SNR G0.9+0.1 with a radio image formed from a reanalysis of the Very Large Array (VLA) observations described by Helfand & Becker (1987). Other than point sources distributed throughout the field, the only emission seen in the *Chandra* data is an extended X-ray source coincident with the central radio PWN. The brightest part of the X-ray nebula is approximately  $1' \times 1'$  in extent and lies within the eastern half of the radio PWN. Fainter X-ray emission is seen to the north, south, and west, the full extent of the X-ray nebula corresponding well to that seen in the radio. No X-ray emission can be seen corresponding to the radio shell of diameter  $7'\text{--}8'$  that surrounds the central nebula.

<sup>1</sup> Center for Space Research, Massachusetts Institute of Technology, 70 Vassar Street, Cambridge, MA 02139; bmg@space.mit.edu.

<sup>2</sup> Hubble Fellow.

<sup>3</sup> Current address: Therma-Wave Inc., 1250 Reliance Way, Fremont, CA 94539.

<sup>4</sup> Department of Astronomy and Astrophysics, Pennsylvania State University, 525 Davey Laboratory, University Park, PA 16802.

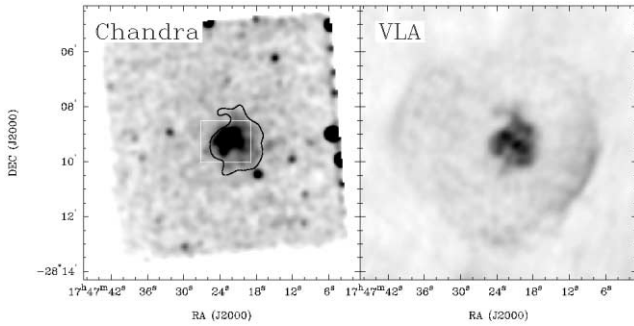


FIG. 1.—X-ray and radio comparison of SNR G0.9+0.1. *Left:* *Chandra* image of the entire S3 chip in the energy range of 0.5–8.0 keV, corrected with an exposure map weighted by the spectrum of the central nebula and then convolved with a Gaussian of FWHM = 15". *Right:* 1.5 GHz VLA image of the same region, with a spatial resolution of 11" × 15". The black contour drawn on the X-ray image corresponds to 1.5 GHz radio emission at the level of 30 mJy beam<sup>-1</sup> and delineates the outer boundary of the radio PWN; the white box marked on the X-ray image shows the extent of the region enclosed by the left panel of Fig. 2.

Figure 2 shows the brighter parts of the X-ray nebula at higher resolution. This region shows a definite axisymmetry, with the reflection axis running at an angle of  $\approx 165^\circ$  (measured counterclockwise from north). Four main features are seen in this region:

1. Near the center of this region is a bright elliptical clump of emission of dimensions 5" × 8". The right panel of Figure 2 shows a higher resolution image of this source, showing a bright region along the southwestern edge of this clump.
2. An unresolved source with a signal-to-noise ratio of  $\sim 4\sigma$  is 10" to the south of this clump. The position of this source is (J2000) R.A. = 17<sup>h</sup>47<sup>m</sup>22<sup>s</sup>.8, decl. = -28°09'15".0, with approximate uncertainties of  $\pm 0''.5$  in each coordinate. In further discussion, we refer to this source as CXOU J174722.8–280915.
3. A semicircular arc of radius 25"–30", which is bisected by the symmetry axis, runs east-west across the nebula.
4. In the southern half of the nebula, an elongated jetlike feature of length 35"–40" lies along the symmetry axis.

After applying a background correction,  $2332 \pm 66$  counts were extracted for the overall nebula, corresponding to a count

TABLE 1  
COUNT RATES AND HARDNESS RATIOS FOR COMPONENTS  
OF THE X-RAY NEBULA

Region	Count Rate <sup>a</sup> (counts ks <sup>-1</sup> )	Hardness Ratio <sup>b</sup>
Entire nebula .....	$67.1 \pm 1.9$	$0.51 \pm 0.05$
Arc .....	$21.0 \pm 1.0$	$0.54^{+0.09}_{-0.08}$
Clump .....	$10.0 \pm 0.6$	$0.49^{+0.12}_{-0.10}$
Jet .....	$3.8 \pm 0.4$	$0.68^{+0.28}_{-0.20}$
CXOU J174722.8–280915 .....	$0.37^{+0.14}_{-0.11}$	$0.54^{+1.05}_{-0.37}$

<sup>a</sup> Count rates are for the energy range of 3–8 keV and have been corrected for background; uncertainties are  $\pm 1\sigma$ .

<sup>b</sup> Defined as the ratio of counts with energies of 5–8 keV to those with energies of 3–5 keV. Uncertainties are all at 90% confidence and have been determined using the formulae given by Gehrels 1986.

rate of  $67.1 \pm 1.9$  counts ks<sup>-1</sup>. Fitting a power-law spectrum to these data implies an absorbing hydrogen column  $N_{\text{H}} = (1.6 \pm 0.2) \times 10^{23}$  cm<sup>-2</sup>, a photon index  $\Gamma = 2.3 \pm 0.4$ , and an unabsorbed flux density in the range of 2–10 keV of  $f_{\text{X}} = (9.6^{+1.7}_{-1.5}) \times 10^{-12}$  ergs s<sup>-1</sup> cm<sup>-2</sup> (all uncertainties  $\pm 1\sigma$ ). For this fit, we find that  $\chi^2 = 123$  for 138 degrees of freedom.

We lack sufficient counts to perform accurate spectral fits to subregions of the nebula. To look for spectral variations, we define the hardness ratio  $H$  to be the ratio of incident counts at energies of 5–8 keV to those with energies of 3–5 keV (less than 5% of the counts from the nebula originate at energies below 3 keV). The corresponding count rates and values of  $H$  for the different components are given in Table 1.

The excess of photons along the southwestern edge of the bright central clump suggests the possible presence of an embedded point source. In order to constrain the flux of such a source, we generated a simulated point source at the position of the peak count rate in the clump, at coordinates (J2000) R.A. = 17<sup>h</sup>47<sup>m</sup>22<sup>s</sup>.9, decl. = -28°09'05".6. We then multiplied this point source by a scaling factor and subtracted the result from the image. By steadily increasing the scaling factor until the residual image showed a significant deficit at the position of the simulated point source, we can put an upper limit of  $\sim 55$  counts on the contribution from such a source, corresponding to a maximum count rate of 1.6 counts ks<sup>-1</sup>. This brightness enhancement is only seen at high energies; for the 11 photons falling at the peak position within the clump, the hardness ratio is  $H = 4.5^{+24.3}_{-3.4}$  (where uncertainties are at 90%

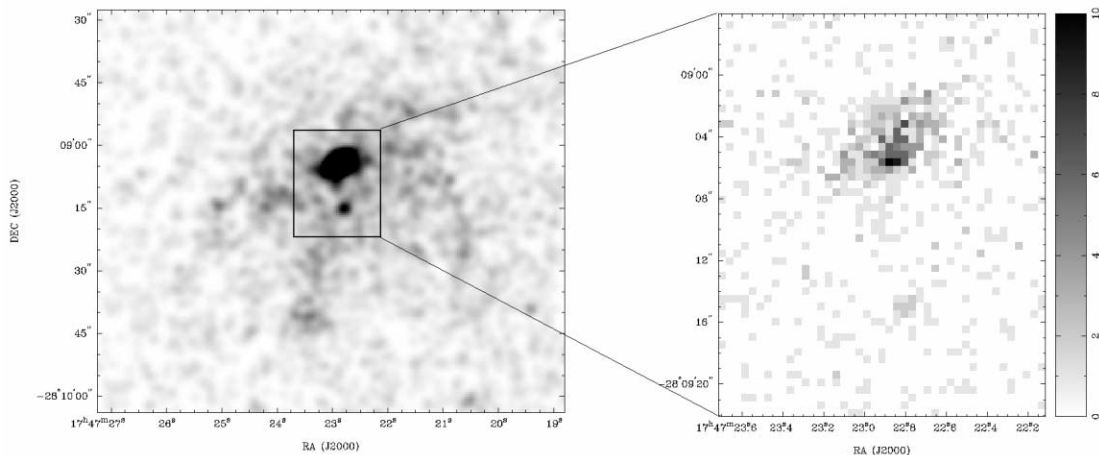


FIG. 2.—*Chandra* observations of the X-ray PWN within SNR G0.9+0.1 in the energy range of 3.0–8.0 keV. *Left:* Inner region of the nebula, exposure-corrected and then smoothed with a Gaussian of FWHM = 3". *Right:* Central clump and unresolved source (CXOU J174722.8–280915) within this inner region. No exposure correction or smoothing has been applied to this latter image; the scale shown at right is in units of raw counts.

confidence and have been derived using the prescription of Gehrels 1986).

#### 4. DISCUSSION

The overall morphology of the X-ray nebula matches that of the radio nebula, making it certain that we have detected X-ray emission from the PWN associated with G0.9+0.1. Our spectral fit to the overall nebula is comparable to that obtained by Sidoli et al. (2000), although with values of  $N_{\text{H}}$ ,  $\Gamma$ , and  $f_{\text{X}}$  all 1–2  $\sigma$  higher than for the *BeppoSAX* data. The region of brightest X-ray emission (shown in the right panel of Fig. 2) is offset from the central peak of the radio PWN by  $\sim 30''$  to the northeast. This presumably reflects a change in the nebular conditions on a timescale intermediate between the X-ray and radio synchrotron lifetimes. Specifically, this offset is most likely due either to motion of the pulsar away from its birth site or to interaction between the PWN and the SNR reverse shock (Chevalier 1998).

The hardness ratios listed in Table 1 provide no evidence for any significant spectral variations in the PWN; the “jet” feature has a higher hardness ratio than the rest of the PWN, but only at the 1  $\sigma$  level. As a point of reference, we find empirically that for the region of the CCD that we are considering, a power-law spectrum with absorbing column  $N_{\text{H}} = 1.5 \times 10^{23} \text{ cm}^{-2}$  and hardness ratio  $H$  has a photon index  $\Gamma \approx (4.8\text{--}5)H$ . The values of  $H$  for all components are therefore consistent with the mean photon index  $\Gamma = 2.3$  inferred from spectral fitting.

We are unable to derive an upper limit on the flux for the shell component of the SNR: the shell (as delineated by its radio morphology) fills the entire CCD, so that a background correction is not possible. However, given the high absorbing column measured toward the PWN, it is unlikely that any thermal emission from the SNR shell is detectable. This can be demonstrated by considering the young ( $\leq 2000$  yr) and X-ray bright [ $L_{\text{X}}(1\text{--}10 \text{ keV}) \approx 3 \times 10^{35} \text{ ergs s}^{-1}$ ] SNR G27.4+0.0 (Kes 73), which has an X-ray spectrum approximated by thermal bremsstrahlung at a temperature  $kT = 0.8 \text{ keV}$  (Gotthelf & Vasisht 1997). If we assume this same spectrum for the shell of G0.9+0.1, then at a distance of 10 kpc and for a foreground column  $N_{\text{H}} \approx 1.5 \times 10^{23} \text{ cm}^{-2}$ , the expected count rate for the S3 CCD is  $\approx 31 \text{ counts ks}^{-1}$  in the energy range of 0.5–8 keV. Thus, even if the shell is as bright as that for G27.4+0.0, we expect it to produce only  $\sim 1000$  counts spread over the entire CCD. This would not be detectable when compared with the 20,000–30,000 background counts accumulated over the same area.

##### 4.1. A Central Pulsar?

X-ray observations of PWNs often reveal the pulsar itself, in the form of a centrally located point source. In the case of G0.9+0.1, there are two possible locations for such a source—the unresolved source CXOU J174722.8–280915 and a possible point source embedded in the clump 10'' to the north of this.

Unlike most of the point sources seen elsewhere in the field, CXOU J174722.8–280915 is only seen at energies above 3 keV, indicating that it is highly absorbed. We can thus rule out the possibility that CXOU J174722.8–280915 is a foreground star. We next consider the possibility that CXOU J174722.8–280915 is a background active galactic nucleus. Adopting a power-law spectrum of photon index  $\Gamma = 1.2$  (Mushotzky et al. 2000) and an absorbing column  $N_{\text{H}} \approx 2 \times 10^{23} \text{ cm}^{-2}$  through the entire Galaxy, the count rate measured

for CXOU J174722.8–280915 corresponds to an unabsorbed 2–10 keV flux density of  $\sim 6 \times 10^{-14} \text{ ergs cm}^{-2} \text{ s}^{-1}$ . There are approximately 20–50 background sources per square degree of this flux density or greater (Mushotzky et al. 2000; Tozzi et al. 2001); the probability of one such source falling within the boundaries of the X-ray PWN by chance is  $\sim (6\text{--}14) \times 10^{-3}$ . We thus think it likely that CXOU J174722.8–280915 is associated with the PWN and the SNR.

If CXOU J174722.8–280915 is a young central pulsar, we expect the X-ray emission from it to correspond either to non-thermal emission from the magnetosphere or to modified blackbody emission from the neutron star surface (e.g., Becker & Trümper 1997). We first consider a blackbody spectrum: a neutron star of age  $10^3\text{--}10^4$  yr is expected to have a surface temperature  $kT \approx 0.1 \text{ keV}$  (e.g., van Riper, Link, & Epstein 1995), which, for  $N_{\text{H}} = 1.5 \times 10^{23} \text{ cm}^{-2}$ , corresponds to  $H = 2 \times 10^{-8}$ , clearly in disagreement with the observed value of  $H = 0.54^{+1.05}_{-0.37}$ . Invoking an extremely high temperature of  $kT = 1 \text{ keV}$  gives  $H = 0.4$  but requires a very small emitting area (inferred blackbody radius of 70 m) in order to match the observed count rate. Alternatively, if we assume a power-law spectrum for the emission from CXOU J174722.8–280915, then for  $\Gamma = 1.5$  (typical for magnetospheric emission; Becker & Trümper 1997) and  $N_{\text{H}} = 1.5 \times 10^{23} \text{ cm}^{-2}$ , we expect a hardness ratio  $H = 0.67$ , in good agreement with the value in Table 1. From the limited spectral information available, we therefore conclude that the X-rays from CXOU J174722.8–280915 are most likely nonthermal in origin. For a distance  $10d_{10}$  kpc, the isotropic unabsorbed luminosity for the source is then  $\sim 6 \times 10^{32} d_{10}^2 \text{ ergs s}^{-1}$  in the energy range of 2–10 keV.

The possibility that the pulsar is embedded in the clump 10'' to the north of CXOU J174722.8–280915 must also be considered, especially given the fact that the brightest part of the clump has an unusually hard spectrum. While magnetospheric emission from an embedded pulsar ( $\Gamma = 1.5$ ) should indeed have a harder spectrum than the surrounding nebula ( $\Gamma = 2.3$ ), the expected hardness ratio at this position is  $0.49 < H < 0.61$  for the upper limit on the point-source count rate that we determined in § 3. This is significantly lower than the value of  $H = 4.5^{+24.3}_{-3.4}$  determined at the brightest point in the clump, suggesting that this bright region is not an embedded point source but rather represents unresolved structure and/or statistical fluctuations within this region.

In summary, CXOU J174722.8–280915 provides the only clear evidence for a hard point source within the PWN, and we therefore consider this source to be the best candidate for emission from a central pulsar. In this case, we expect its X-ray emission to be strongly pulsed at the pulsar spin period; unfortunately, our data lack the time resolution and sensitivity to test this hypothesis. The X-ray luminosity of CXOU J174722.8–280915 is  $\sim 0.5\%$  of the total X-ray luminosity of the PWN in the energy range of 2–10 keV, which is somewhat lower than the ratio of magnetospheric pulsar emission to surrounding nebular emission seen in PWNs whose pulsars have been identified (Becker & Trümper 1997).

##### 4.2. Nebular Morphology

The X-ray morphology of the PWN is strikingly axisymmetric. This symmetry axis presumably reflects the orientation of its associated pulsar and likely indicates either the direction of the pulsar’s motion or the orientation of the pulsar spin axis.

In the former case, the pulsar’s projected direction of motion is presumably in the direction  $15^\circ$  west of north, and the semi-circular arc represents a bow shock produced where the pulsar

wind comes into pressure equilibrium with surrounding material. However, it is then difficult to understand the jetlike feature extending to the south of CXOU J174722.8–280915. The radio/X-ray spectrum of the PWN shows a steepening at a frequency  $\nu_b \sim 10^{11}$ – $10^{12}$  Hz (Sidoli et al. 2000); if this spectral break results from synchrotron cooling, then electrons emitting at a frequency  $\nu = \nu_b$  must have a radiative lifetime  $t_r \sim \tau = 1$ –7 kyr. Since  $t_r \propto \nu^{-1/2}$ , electrons emitting at 5 keV must have a synchrotron lifetime  $t_r \sim (3$ – $10) \times 10^{-4} \tau \sim 0.3$ –7 yr. Even for an extreme velocity  $V \sim 2000$  km s $^{-1}$ , the pulsar can only travel less than 1% of the length of the jetlike feature in this short time. The jetlike feature therefore cannot correspond to a wake of synchrotron-emitting particles and has no clear explanation within the bow-shock interpretation. Furthermore, we expect the bow-shock morphology to be clearly apparent at radio wavelengths, as is seen for the PWNs around other high-velocity pulsars (e.g., Frail et al. 1996; Olbert et al. 2001). However, it is clear from Figure 1 that in this case, the radio emission is amorphous and clearly extends well to the north of the X-ray arc. We therefore think a bow shock to be an unlikely interpretation of the data.

The alternative is that the X-ray nebula’s symmetry axis corresponds to the pulsar spin axis. Such a possibility has been proposed for the PWNs associated with the Crab and Vela pulsars (Hester et al. 1995; Helfand, Gotthelf, & Halpern 2001) and possibly also for PSR B1509–58 and B0540–69 (Brazier & Becker 1997; Gotthelf & Wang 2000). In all these cases, it has been argued that the pulsar’s X-ray PWN has two main components: (1) a torus representing the region where an equatorially concentrated wind terminates and shocks and (2) a pair of jets running perpendicular to this torus that correspond to a collimated wind directed along the pulsar spin axis.

At the available sensitivity and resolution, it is reasonable to propose that the X-ray PWN within SNR G0.9+0.1 has a similar underlying morphology: the semicircular arc can be interpreted as half of an equatorial torus, while the elongated feature running along the symmetry axis would then be a polar jet. In this interpretation, the pulsar is expected to lie at the center of the arc and along the jet; the fact that CXOU J174722.8–280915 sits at this position supports the argument that this point source is indeed the pulsar.

If the torus is circular when viewed along the polar axis, its ratio of projected minor to major axes of  $\sim 0.75$  (as measured from the left panel of Fig. 2) implies an inclination of the pulsar spin axis to the line of sight of  $\theta \sim 40^\circ$ . The radius of the torus is then  $R \sim 1.2d_{10}$  pc, and the length of the jet is  $L \sim 2.5d_{10}$  pc. The absence of the other half of the torus and of a counterjet, as are seen also for the PWN around the Vela pulsar (Helfand et al. 2001), can be accounted for by Doppler boosting: for wind speeds greater than  $c/3$  (Kennel & Coroniti 1984) and  $\Gamma = 2.3$ , the approaching components of the jet (torus) will be boosted to a brightness a factor  $r > 6$  ( $r > 4$ ) over receding material. The observed ratios of surface bright-

ness of the jet and arc compared with any counterjet and counterarc, respectively, are both  $r \gtrsim 5$ , consistent with this interpretation. The light-travel time along the jet is  $\sim 8d_{10}$  yr. Provided that  $d_{10} \lesssim 1$  and that the outflow velocity is close to  $c$ , this is consistent with the upper end of the range of synchrotron-emitting lifetimes inferred above.

The scale of features seen in this PWN is considerably larger than for the nebulae around the Crab ( $R \sim 0.4$  pc,  $L \sim 0.6$  pc; Hester et al. 1995) or Vela ( $R \sim 0.03$  pc,  $L \sim 0.01$  pc; Helfand et al. 2001)<sup>5</sup> pulsars but are comparable to that of the X-ray PWN surrounding PSR B1509–58, ( $R \sim 1.5$  pc,  $L > 7$  pc; Brazier & Becker 1997; Tamura et al. 1996). In this latter case, the large extent of the PWN is thought to be due to the low-density environment ( $n \lesssim 0.01$  cm $^{-3}$ ; Bhattacharya 1990; Gaensler et al. 1999). A similar low density for G0.9+0.1 is consistent with its faint radio shell.

The bright clump seen to the north of CXOU J174722.8–280915 cannot be explained within the context of a “torus + jets” geometry. The clump is clearly a discrete structure superposed on the fainter nebular background and is not a geometric effect resulting from overlapping emission from torus and jet components. The fact that the clump is offset slightly to the east of the symmetry axis and is elongated along a different axis to that of the PWN suggests that it is not part of the overall axisymmetric structure; it may represent an intermediate-latitude feature where the pulsar wind is shocked or compressed. Such compact features may be highly time-variable, as has been seen in optical and X-ray observations of the Crab and Vela PWNs, respectively (Hester 2001; Pavlov et al. 2001).

Regardless of any detailed interpretation for the nebular morphology seen here, the data demonstrate that the flow of energy away from the central pulsar in SNR G0.9+0.1 is distinctly anisotropic and add support to the hypothesis that axial/equatorial wind morphologies are generic among the pulsar population. It is clear that the high spatial resolution now available in X-rays with *Chandra* can play an important role in determining how young pulsars deposit their energy into their environments.

We are grateful to Mark Bautz and the ACIS Team for inviting us to work on this project, and we thank Fred Baganoff, Dave Pooley, and Pat Slane for useful discussions. B. M. G. acknowledges the support of NASA through Hubble Fellowship grant HST-HF-01107.01-A awarded by the Space Telescope Science Institute. M. J. P. acknowledges the support of NASA contracts NAS8-37716 and NAS8-38252.

<sup>5</sup> The jet that we refer to in the case of the Vela pulsar is the 10” long feature aligned with the pulsar spin axis. A much longer “jet” has been reported by Markwardt & Ögelman (1995) but does not form part of the axisymmetric morphology of the inner X-ray nebula.

#### REFERENCES

- Bautz, M. W., et al. 1998, *Proc. SPIE*, 3444, 210  
 Becker, W., & Trümper, J. 1997, *A&A*, 326, 682  
 Bhattacharya, D. 1990, *J. Astrophys. Astron.*, 11, 125  
 Brazier, K. T. S., & Becker, W. 1997, *MNRAS*, 284, 335  
 Burke, B. E., Gregory, J., Bautz, M. W., Prigozhin, G. Y., Kissel, S. E., Kosicki, B. N., Loomis, A. H., & Young, D. J. 1997, *IEEE Transac. Electron Devices*, 44, 1633  
 Chevalier, R. A. 1998, *Mem. Soc. Astron. Italiana*, 69, 977  
 Frail, D. A., Giacani, E. B., Goss, W. M., & Dubner, G. 1996, *ApJ*, 464, L165  
 Gaensler, B. M. 2001, in *AIP Conf. Proc.* 565, *Young Supernova Remnants*, ed. S. S. Holt & U. Hwang (New York: AIP), 295  
 Gaensler, B. M., Brazier, K. T. S., Manchester, R. N., Johnston, S., & Green, A. J. 1999, *MNRAS*, 305, 724  
 Gehrels, N. 1986, *ApJ*, 303, 336  
 Gotthelf, E. V., & Vasisht, G. 1997, *ApJ*, 486, L133  
 Gotthelf, E. V., & Wang, Q. D. 2000, *ApJ*, 532, L117  
 Helfand, D. J., & Becker, R. H. 1987, *ApJ*, 314, 203  
 Helfand, D. J., Gotthelf, E. V., & Halpern, J. P. 2001, *ApJ*, in press (astro-ph/0007310)

- Hester, J. J. 2001, in AIP Conf. Proc. 565, Young Supernova Remnants, ed. S. S. Holt & U. Hwang (New York: AIP), 285
- Hester, J. J., et al. 1995, ApJ, 448, 240
- Høg, E., Kuzmin, A., Bastian, U., Fabricius, C., Kuimov, K., Lindegren, L., Makarov, V. V., & Roeser, S. 1998, A&A, 335, L65
- Kennel, C. F., & Coroniti, F. V. 1984, ApJ, 283, 694
- Markwardt, C. B., & Ögelman, H. 1995, Nature, 375, 40
- Mereghetti, S., Sidoli, L., & Israel, G. L. 1998, A&A, 331, L77
- Mushotzky, R. F., Cowie, L. L., Barger, A. J., & Arnaud, K. A. 2000, Nature, 404, 459
- Olbert, C. M., Clearfield, C. R., Williams, N. E., Keohane, J. W., & Frail, D. A. 2001, ApJ, 554, L205
- Pavlov, G. G., Kargaltsev, O. Y., Sanwal, D., & Garmire, G. P. 2001, ApJ, 554, L189
- Sidoli, L., Mereghetti, S., Israel, G. L., & Bocchino, F. 2000, A&A, 361, 719
- Tamura, K., Kawai, N., Yoshida, A., & Brinkmann, W. 1996, PASJ, 48, L33
- Tozzi, P., et al. 2001, ApJ, in press (astro-ph/0103014)
- van Riper, K. A., Link, B., & Epstein, R. I. 1995, ApJ, 448, 294